RESEARCH ARTICLE
SPACE PHYSICS: IONOSPHERIC PHYSICS

Earth and Planetary Physics
8: 391–399, 2024
doi: 10.26464/epp2024010

Overshoot phenomena: Observation and simulation

Ting Feng, MoRan Liu*, ShiMin He, Xiang Wang, and Chen Zhou

Department of Space Physics, School of Electronic Information, Wuhan University, Wuhan 430072, China

Key Points:

- The competition between PDI and OTSI leads to the first peak in the initial stage of overshoot, which we name pre-miniovershoot.
- The ion density cavitons generation and collapse following the pre-miniovershoot contribute to the miniovershoot phenomenon.
- The mechanism in the pre-miniovershoot, miniovershoot and mainovershoot has been discussed.

Citation: Feng, T., Liu, M. R., He, S. M., Wang, X., and Zhou, C. (2024). Overshoot phenomena: Observation and simulation. *Earth Planet. Phys.*, *8*(2), 391–399. http://doi.org/10.26464/epp2024010

Abstract: High-power O-mode radio waves can excite artificial instabilities in the F region, according to experiments conducted at the European Incoherent Scatter Science Association (EISCAT) heating facility. The main instabilities include the parametric decay instability (PDI), oscillating two-stream instability (OTSI), and thermal parametric instability (TPI). The PDI and OTSI not only compete with each other, but also compete with the TPI, leading to a two-stage overshoot phenomenon: a miniovershoot occurs on a millisecond time scale after pump-on, followed by the main overshoot. We gain insight into the miniovershoot via a generalized Zakharov model, whereas the main overshoot can be observed as an enhanced plasma line overshoot phenomenon in incoherent scatter radar spectra. We can also observe that the zero-frequency ion line exists only in the initial heating period after a cold start and that the upshifted and downshifted ion lines behave irregularly in the spectra. The simulation results show that competition between the PDI and OTSI leads to an initial peak, which we named the pre-miniovershoot. The following processes, namely ion density caviton generation, and collapse and cascade in the development of the PDI, contribute to the miniovershoot phenomenon.

Keywords: overshoot; parametric decay instability; oscillating two-stream instability; competition

1. Introduction

High-power O-mode (ordinary pump wave) heating experiments can effectively excite a parametric decay instability (PDI) and oscillating two-stream instability (OTSI) near their reflection height (Perkins et al., 1974; Stubbe et al., 1992). In the PDI, the pump wave decays into a downward Langmuir wave and an upward ion acoustic wave, that is, a three-wave interaction (Fejer, 1979). The PDI saturates within a few milliseconds after the transmitter is initially switched on (Hagfors et al., 1983; Djuth et al., 2004) and gives rise to the enhanced plasma lines observed by incoherent scatter radars (ISRs; Stubbe et al., 1992). The OTSI is also called a purely growing instability, in which the pump wave decays into two Langmuir waves propagating in opposite directions and a nonpropagating ion acoustic wave, that is, a four-wave interaction (Robinson, 1997).

These instabilities not only compete with each other (DuBois et al., 1992; Chian and Rizzato, 1994) but also have to contest with those that occur in the upper hybrid (UH) resonance region (Kuo SP, 2001), such as the thermal parametric instability (TPI). The height of the UH resonance region is a few kilometers (2 to 5 km) below the pump wave reflection altitude (Kotov et al., 2007). The excitation threshold of the OTSI is higher than that of the PDI (Kuo SP, 2001), but the OTSI has a greater linear growth rate than does the PDI (Mahmoudian et al., 2017). Nevertheless, the intensity of the PDI, as indicated by the saturated amplitude of the electric field, is always greater than that of the OTSI (Showen and Kim, 1978). Otherwise, the PDI and OTSI have to compete with the instabilities excited at the UH resonance region (Kuo SP et al., 1997). These two kinds of competition lead to a two-stage process of overshoot phenomena: a miniovershoot on a time scale of 10 ms, and a main overshoot on a time scale of 100 ms (Showen and Kim, 1978). The overshoot comprises two evident enhancements, namely the miniovershoot and the main overshoot, observed in the plasma line spectra when the high-frequency (HF) power is abruptly switched on. Additionally, Frolov et al. (2004) used a short-time and long-time overshoot to reflect their physical nature, namely the ponderomotive and thermal plasma processes.

Langmuir waves develop and saturate within a few milliseconds after the transmitter is turned on, and they remain until ion density cavitons begin to develop and collapse, leading to the miniovershoot (Muldrew, 1988). Frolov et al. (2004) provided another possible cause of the miniovershoot, that is, the generation of small-scale striations during the stage of ponderomotive instability development. Nevertheless, the physical mechanism of the

First author: T. Feng, tingfeng@whu.edu.cn
Correspondence to: M. R. Liu, moranliu@whu.edu.cn
Received 04 AUG 2023; Accepted 11 JAN 2024.
First Published online 29 FEB 2024.

miniovershoot is not yet completely understood (Frolov et al., 2004). Two reasonable explanations have been proposed for the existence of the valley region between the miniovershoot and the main overshoot in ~10–30 ms: the excited PDI removes evident energy from the pump wave, or part of the energy in the pump wave is transferred to a slower and unstable Langmuir wave (Muldrew, 1988). For ~30–200 ms, the ponderomotive force of the trapped Langmuir wave causes a decrease in the electron density, which results in the detection of a larger range of Langmuir waves by ISRs. The Langmuir wave and ion acoustic waves are then quenched by fully established artificial meter-scale field-aligned irregularities (FAIs) generated close to the UH resonance height (Blagoveshchenskaya et al., 2017), which results in the main overshoot. The fully established small-scale FAIs can lead to absorption of the pump wave power to a level below that required to excite the PDI and OTSI (Bryers et al., 2013). The growth time of the PDI and OTSI is a few milliseconds. Otherwise, the growth time for the TPI is on an order of seconds (Robinson, 1983), which is associated with the growth of small-scale FAIs. The time constants associated with the growth of FAIs can only be explained by stimulating a TPI, in which the coupling mechanism is thermal instead of ponderomotive (Robinson, 1983). Additionally, the overshoot normally lasts 1 to 6 s; thus, it can be recognized by ISRs as the first 5 s of enhanced spectra.

The overshoot phenomenon is characterized by an increase and subsequent decrease within a time scale of a few seconds. Robustly HF-enhanced plasma lines (HFPLs) and HF-enhanced ion lines (HFILs) designate the transient response from the cold-start O-mode heating after the O-mode pump is on, which can be seen in the first 5 s of spectra (Blagoveshchenskaya et al., 2017). Note that only the Langmuir waves with a wavenumber twice that of the radar signal and propagating parallel or antiparallel to the pointing direction of the radar can be obtained as HFPLs (Kuo SP, 2001).

However, when the effective radiated power (ERP) is high enough, the TPI is suppressed because of the electron temperature dependence (Gustavsson et al., 2009; Feng T et al., 2020). Once the TPI is restrained, the PDI and OTSI begin to compete with each other. This study aims to explore the reappearance of the PDI after the overshoot feature with the absence of the OTSI and to offer full insights into the overshoot phenomenon via ISR spectra and simulation results.

2. Experimental Observations

Here we present two representative O-mode heating experiments performed by the Russian team led by N. F. Blagoveshchenskaya and the Norwegian team led by B. Gustavsson at Tromsø, Norway. The HFPLs and HFILs are observed by the European Incoherent Scatter Science Association (EISCAT) ultra high frequency (UHF; 933 MHz) radar in beata mode with a 5-s integration time and a 3-km range resolution. Figures 1 and 2 show the power-stepping experiment results at 13:12–13:30 universal time (UT) on October 29, 2015, when the heater transmitted a high-powered O-mode pump wave at 7.953 MHz. The power-stepping ERP was 4.8, 13.7, 48.6, 138.8, 289.4, and 547.2 MW. The O-mode HF radio wave is magnetic zenith directed. In Figures 1b, 1d, 1f, and 2c, the existence of the peaks in zero-frequency ion line spectra with the enhanced plasma lines at pump wave frequency indicates the excitation of the OTSI even under smaller ERP, such as 48.6 MW (Dubois et al., 1993). This is the so-called zero-frequency ion line overshoot phenomenon. Meanwhile, the plasma line overshoots are obtained as shown in Figures 1f, 1g, and 2e. However, in the last ERP period, after the overshoot stage, the HFILs and HFPLs (see Figures 2b, 2d, and 2e) are direct evidence of the recovery of the PDI. Further, the upshifted and downshifted ion lines are observed throughout this largest ERP period, unlike the zero-frequency ion line suggesting the absence of the OTSI. A possible inference is that because of the suppression of the TPI, the PDI quickly recovers with the preexistence of the striation formed after heat-on and absorbs the energy of the pump wave, preventing the recovery of the OTSI by taking advantage of its generation altitude. Another explanation is that the electric field threshold of the OTSI strongly depends on the electron temperature,

$$E^2_{\mathrm{OTSI}} = 4\frac{T_\mathrm{e}+T_\mathrm{i}}{T_\mathrm{i}}\frac{n_\mathrm{e}k_\mathrm{B}T_\mathrm{i}\nu}{\omega_\mathrm{p}\epsilon_0},$$

which is different from that of the PDI,

$$E^2_{\mathrm{PDI}} = 4\frac{n_\mathrm{e}k_\mathrm{B}T_\mathrm{i}\nu}{\omega_\mathrm{p}\epsilon_0 B_{\max}}$$

(Bryers et al., 2013), where T_e and T_i are the electron and ion temperatures, ν is the electron collision frequency, and n_e denotes the electron density. The Boltzmann constant is k_B, and ε_0 is the permittivity of free space, whereas $B_{\max}$ is a function of $T_\mathrm{e}/T_\mathrm{i}$ presented in Stubbe et al. (1984). Thus, the OTSI cannot recover when the electron temperature is maintained at a high level.

Figures 3 and 4 illustrate the experimental results from 10:04:50 to 11:29:50 UT on November 27, 2014, when the heater transmitted a high-powered O-mode pump at 6.3 MHz toward the magnetic zenith with a 150-s on and 85-s off cycle. This experiment with ERP ranging from ~261–290 MW during the entire heating period obtained representative O-mode heating results. The high-ERP condition was to ensure that the excitation thresholds of the OTSI and PDI were exceeded. Figures 3c, 3e, 4b, and 4d indicate different amplitudes of upward- and downward-propagating ion acoustic waves. Figures 3d and 4c illustrate that at every first 5 s, the zero-frequency ion lines are strongly enhanced owing to the nonpropagating density irregularities, and the plasma lines enhanced at the pump wave frequency in Figure 3f suggest the generation of the OTSI (Bryers et al., 2013). The zero-frequency ion line only exists in the initial heating period after a cold start, and the upshifted and downshifted ion lines behave irregularly. The PDI and the further decayed Langmuir waves can be observed in Figures 3f, 3g, and 4e. Therefore, the PDI and OTSI are excited regularly by the pump wave, as shown in the first 5 s of HFIL and HFPL spectra. The PDI phenomenon then recovers and becomes dominant in the spectra a few seconds after overshoot, whereas the OTSI does not. Under high ERP, the TPI is suppressed owing to the elevated electron temperature and the PDI keeps appearing and disappearing repeatedly until the pump is turned off, which is a manifestation that the PDI is readily excited with the preexisting striation established after the pump is turned on and that it dominates during the entire heating period.

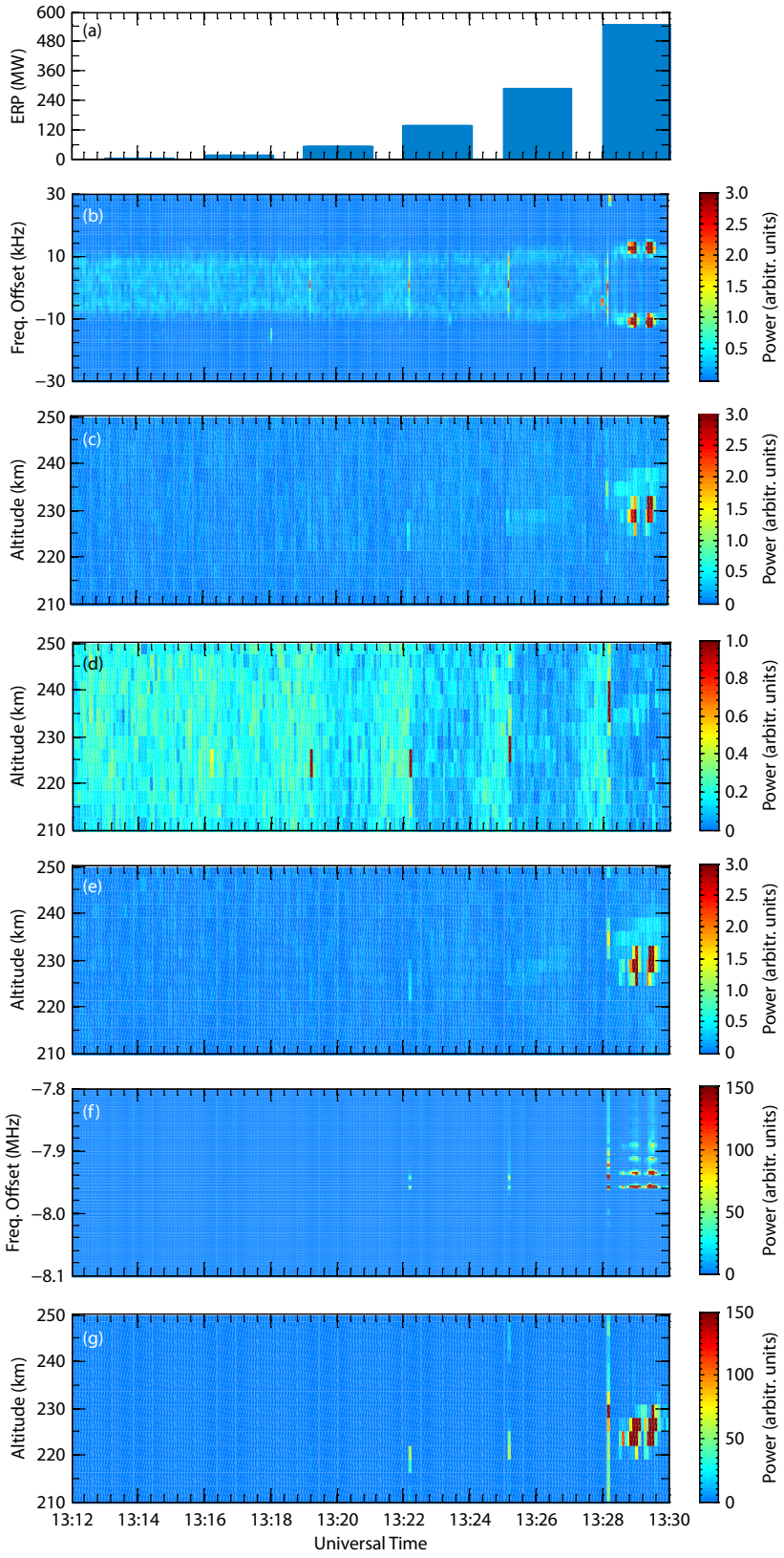

Figure 1. Plasma lines and ion lines observed by EISCAT UHF radar during the power-stepped O-mode ionospheric heating experiment between 13:12 and 13:30 UT on October 29, 2015. (a) Temporal variation of the ERP of O-mode heating; (b) temporal variation of the HFIL in the altitude range of ~224.3–230.2 km; (c) temporal–altitude behavior of the spectra of the upshifted ion line at +10.71 kHz; (d) temporal–altitude behavior of the spectra of the zero-frequency offset ion line; (e) temporal–altitude behavior of the spectra of the downshifted ion line at −10.71 kHz; (f) temporal variation of the downshifted plasma line in the altitude range of ~222.0–227.9 km; (g) temporal–altitude behavior of the spectra of the downshifted plasma line at the pump wave frequency of −7.953 MHz.

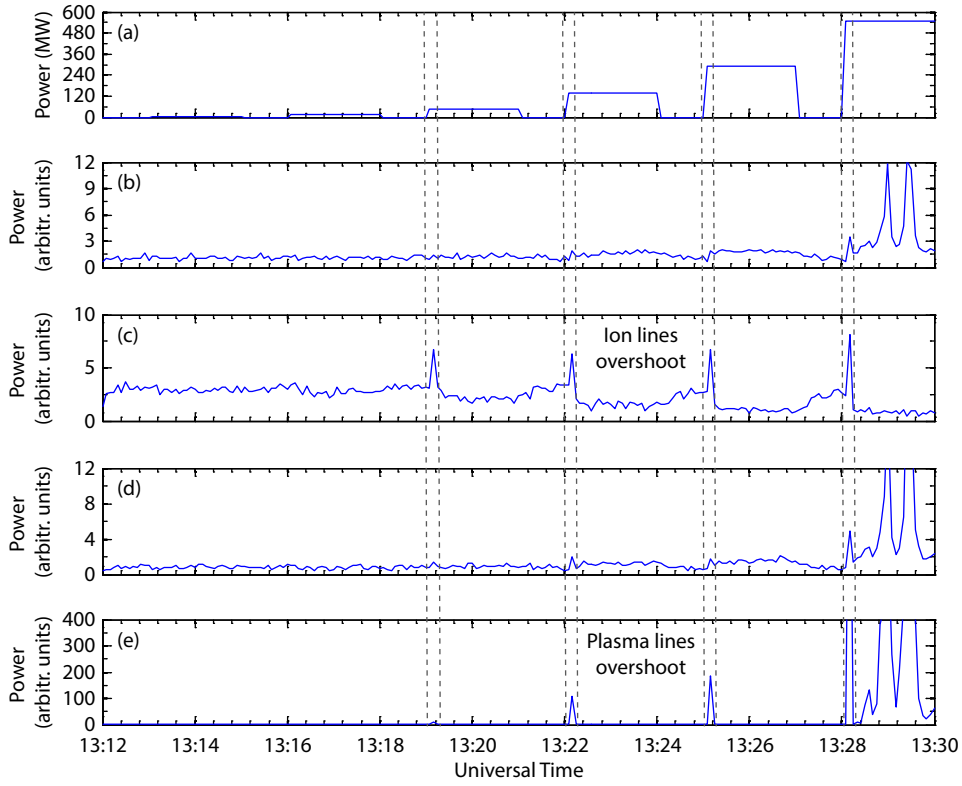

Figure 2. Temporal evolution of HFIL and HFPL power integrated over ~210–250 km during the power-stepped O-mode ionospheric heating experiment between 13:12 and 13:30 UT on October 29, 2015. (a) The ERP of the O-mode pump wave during the entire cycle; (b) the upshifted ion line; (c) temporal behavior of the zero-frequency ion line; (d) the downshifted ion line; (e) the downshifted plasma line. The dashed lines indicate the first 5 s after the transmitter is turned on, marking the occurrence of the overshoot.

3. Simulation

A theoretical model for the temporal evolution of the electric field in ionospheric O-mode heating is used. This model is based on a nonuniform nest grid algorithm proposed by Eliasson (2008) using a generalized Zakharov model. The HF field is coupled to the low-frequency electrostatic fluctuations by the ponderomotive force in this model. The simulation details can be found in Eliasson (2008) and Eliasson et al. (2015). The propagation of the O-mode pump wave is computed via the finite-difference time-domain method in the simulation, which is different from Eliasson's model (Cannon and Honary, 2015). Another difference comes in the calculation of the ponderomotive force with an HF time scale in that we use the mean value instead of the envelope value. We use this model for investigating the competition mechanism between the OTSI and PDI, which may be a proper explanation for the miniovershoot. The threshold for the PDI is readily exceeded (Ashrafi et al., 2007), and that of the OTSI is higher (0.44/0.49 V/m for pump wave frequencies of 5.423 and 6.77 MHz at Tromsø; Kuo SP, 2015). Therefore, the initial electric field is set at 1 V/m to ensure the excitation of the PDI and OTSI, which is set at the bottom of the calculation domain (approximately 2.5 km below the reflection altitude). The special step is set at 4 cm in this model.

Figures 5 to 7 present the results of the simulation. In Figure 5, we can observe the standing wave pattern of the parallel electric field in the initial stage of the simulation. Further, the cavitons associated with the Langmuir turbulence are generated at ~4.036 ms in two separate regions, ~2228.184–2506.712 m and ~1671.128–2088.92 m. As time increases, the standing wave pattern in the lower region collapses and the height of the excited Langmuir turbulence decreases.

In Figure 6, the manifestation of the OTSI and PDI is shown in the frequency spectra rather than the enhanced zero-frequency ion line and plasma line spectra. The black line in this figure is the frequency spectra of the initial ion acoustic wave in the PDI obtained by $f_{\mathrm{IA}} = \dfrac{kC_s}{2\pi}$.

Equations

$$C_s = [k_B(T_e + 3T_i)/m_i]^{1/2}$$

and

$$k = \frac{-2\omega_0 C_s + \sqrt{6v_{th}^2(\omega_0^2 - \omega_p^2) + 4C_s^2\omega_p^2}}{6v_{th}^2 - 2C_s^2}$$

are the speed and wavenumber of the ion acoustic wave, respectively, whereas m_i is the ion mass, v_{th} is calculated by $v_{th} = \sqrt{2k_BT_e/m_e}$, ω_0 is the pump wave frequency, and $\omega_p = \sqrt{(n_0e/\epsilon_0 m_e)}$ is the plasma frequency. In the PDI, the Langmuir wave becomes a mother wave and leads to a cascading process. In this process, the mother Langmuir wave further decays into an ion acoustic wave and another lower frequency Langmuir wave, which results in the extension of the frequency spectra (Ashrafi et al., 2007). Further, the cascading leads to the generation of ion density cavitons and

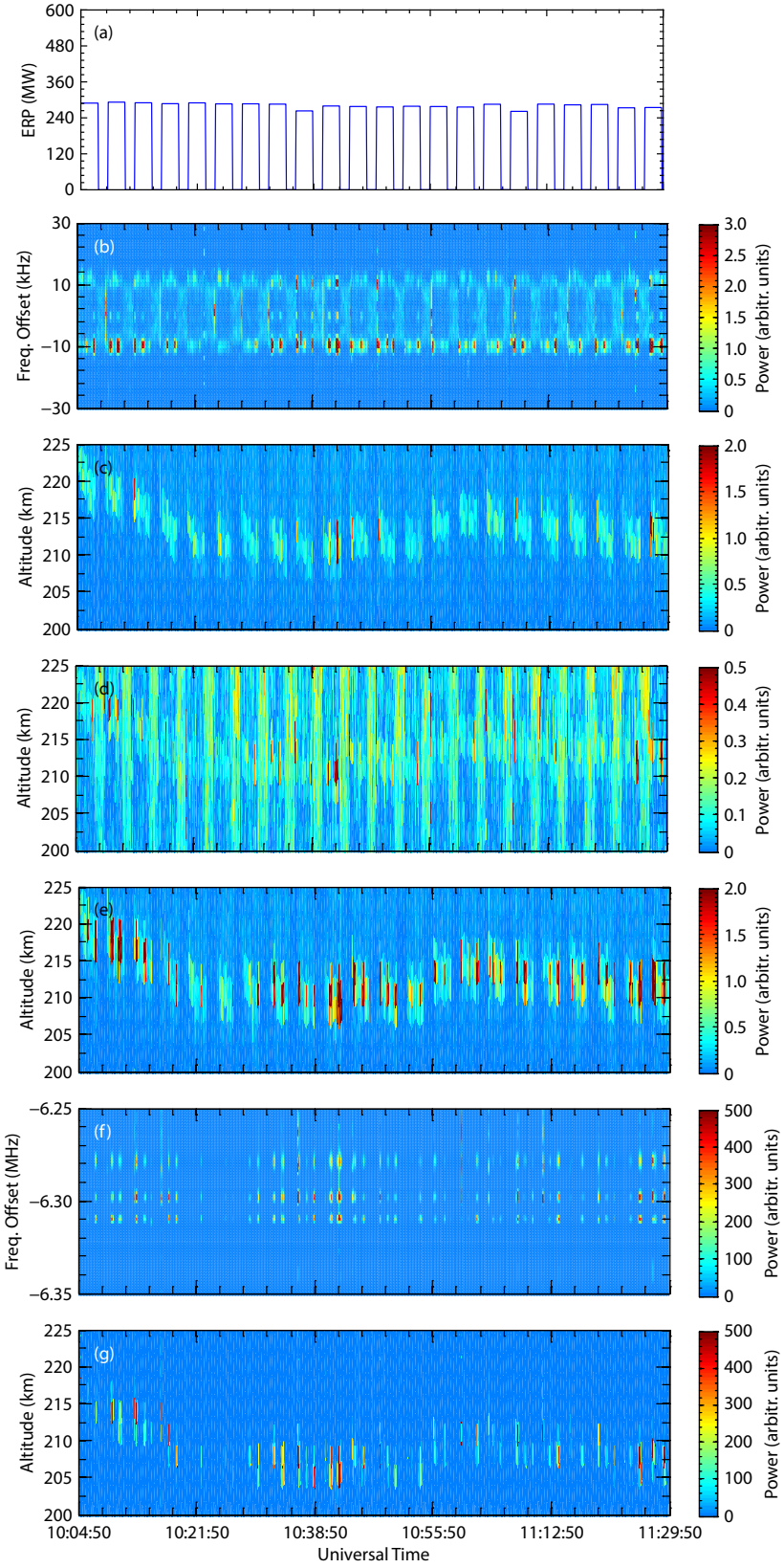

Figure 3. Plasma lines and ion lines observed by EISCAT UHF radar during the O-mode ionospheric heating experiment between 10:04:50 and 11:29:50 UT on November 27, 2014. (a) The pump wave heating period; (b) temporal variation of the HFIL in the altitude range of ~209.3–215.2 km; (c) temporal–altitude behavior of the spectra of the upshifted ion line at +10.71 kHz; (d) temporal–altitude behavior of the spectra of the zero-frequency offset ion line; (e) temporal–altitude behavior of the spectra of the downshifted ion line at −10.71 kHz; (f) temporal variation of the downshifted plasma line in the altitude range of ~203.4–209.3 km; (g) temporal–altitude behavior of the spectra of the downshifted plasma line at the pump wave frequency of −6.3 MHz.

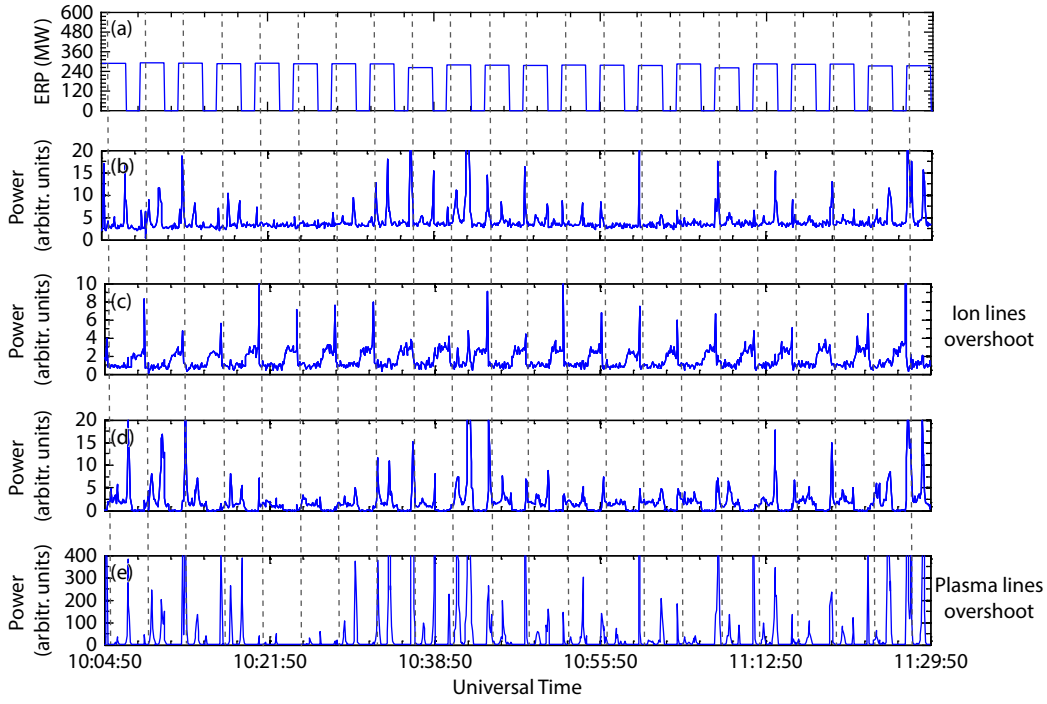

Figure 4. Temporal evolution of HFIL and HFPL power integrated over ~200–230 km during the O-mode ionospheric heating experiment with the ERP ranging from ~260–290 MW between 10:04:50 and 11:29:50 UT on November 27, 2014. (a) The O-mode pump wave heating period during the entire cycle; (b) the upshifted ion line; (c) temporal behavior of the zero-frequency ion line; (d) the downshifted ion line; (e) the downshifted plasma line. The dashed lines indicate the first 5 s after the transmitter is turned on, marking the occurrence of the overshoot.

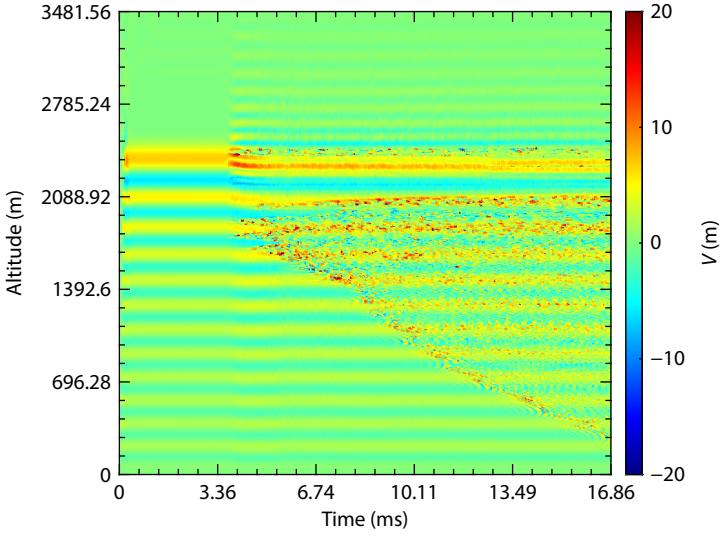

Figure 5. Simulation result of the parallel electric field in the region of z = ~0–3481.56 m.

the following collapse (Streltsov et al., 2018). This process is consistent with spectral lines marked by primary decay and cascade, as shown in Figure 6. Additionally, we can see that the instability excited in the higher region is the OTSI, whereas the PDI is generated at the lower heights corresponding to the separate regions in Figure 5.

Figure 7 illustrates the temporal–altitude behavior of the ion energy spectra $<|n(\boldsymbol{k})|^2>$. During the initial stage, the OTSI grows at a greater rate than the PDI, resulting in the rapid development of the OTSI and the depletion of most of the energy from the heater wave. During this time, the OTSI dominates the heating process, and the subsequent generation of cavitons with the collapse of waves leads to a small peak. This peak is called a pre-miniovershoot and can be seen in the upper panel of Figure 7. With the increase in heating time, the PDI progresses into a cascade process, which results in the development of Langmuir turbulence and contributes to the miniovershoot observed at around 5 ms. This miniovershoot shows a significant consumption of energy from the heater wave and the dominance of the PDI cascade process. Simultaneously, the PDI takes advantage of the

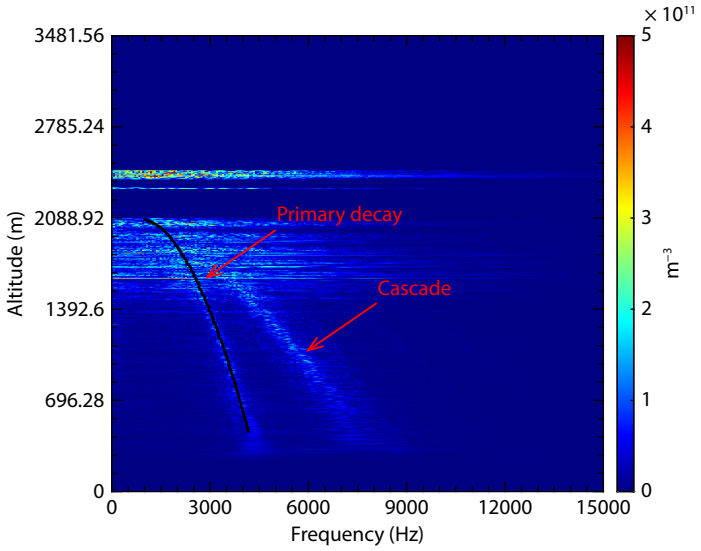

Figure 6. Simulation result of ion density spectra. The primary decay (black line) and cascade of the PDI are marked by the red arrows.

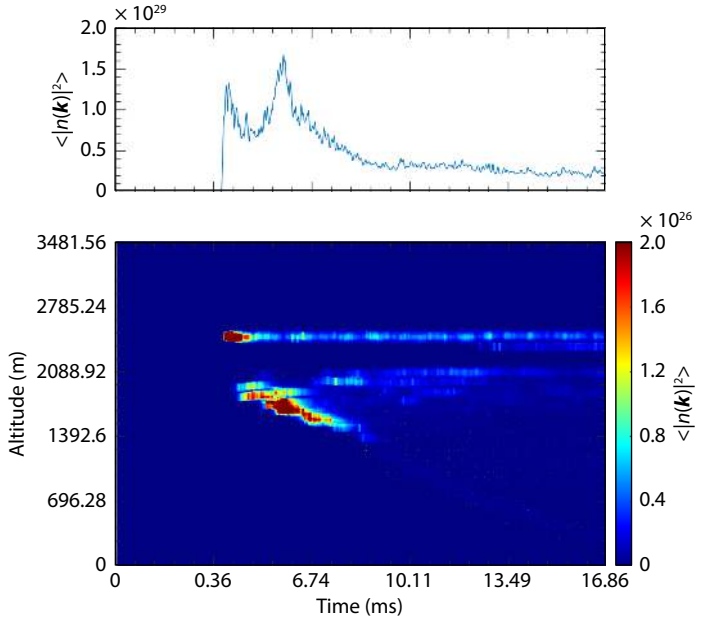

Figure 7. (Top) Simulation result of the ion energy spectra $<|n(\boldsymbol{k})|^2>$ integrated over the computation region. (Bottom) Temporal–altitude behavior of the ion energy spectra.

occurring altitude and temporally prevents the excitation of the OTSI at higher altitudes. The pump wave is scattered by the striations, resulting in reduced power available to drive the PDI and causing the OTSI to diminish. Consequently, this leads to a weakening of the ion acoustic waves. Further, Langmuir waves generated by the PDI are trapped in the cavitons, and the waves begin to collapse after the generation of the miniovershoot, which results in a descending layer, as shown in the bottom panel of Figure 7. In addition, the heating pump power is drained in the PDI-excited region before reaching the OTSI height as the heating time increases.

4. Discussion

Typically, the generated heights of the PDI, OTSI, and TPI are different: $H_{\rm TPI} < H_{\rm PDI} < H_{\rm OTSI}$. The TPI typically develops during the initial pump-on period of 0.5–10.0 s at 2 to 5 km below the reflection height (Perkins et al., 1974; Thidé et al., 2005). Kuo SP (2021) reported that the OTSI and PDI occur near the HF pump wave reflection height; nevertheless, their dispersion functions suggest that the excitation layer of the OTSI is higher and narrower than that of the PDI (Stubbe et al., 1992). Likewise, the HFPL- and HFIL-detected altitudes are governed by the dispersion relations of Langmuir and ion acoustic waves, respectively (Wu J et al., 2019; 2021).

The competitive process between these ponderomotive instabilities and the TPI leads to the main overshoot phenomena (Lee and Kuo SP, 1983). Specifically, the PDI and OTSI are normally quenched within seconds because of the fully established artificial FAIs excited by the TPI under high-power conditions, which scatter

the pump wave, thereby preventing further excitation of the PDI (Stubbe, 1996). In addition, the OTSI, with a higher excitation threshold, is suppressed by instabilities draining the pump wave energy in the UH resonance region (Stubbe et al., 1992). The TPI restrains further development of the OTSI and PDI, resulting in the main overshoot, which is in accordance with the explanation that the FAIs scatter the pump wave before it can arrive at the parametric resonance altitude (Das and Fejer, 1979).

Unlike the explanation of the miniovershoot proposed by Muldrew (1988), we offer insights into another mechanism, that is, that the competition between the PDI and OTSI results in the pre-miniovershoot. This mechanism, along with the ion density caviton generation and collapse, contributes to the miniovershoot, which is close to the assumption of Frolov et al. (2004). The miniovershoot cannot be observed by ISRs owing to the technical limitations of the facility; therefore, we use the model presented above to confirm this inference. According to the simulation results, with the absence of the instabilities occurring at the UH resonance height and taking advantage of the occurring altitude, the PDI will dominate and deplete the heater wave power. The competition between the OTSI and PDI and the wave collapse contribute to the first peak (pre-miniovershoot) and the miniovershoot feature.

Figures 1 to 4 suggest that the temporal behavior of the PDI and OTSI is repeatable once the TPI is suppressed under the high-ERP condition. After the overshoot, the striation is well developed, so the PDI only needs a lower power to be excited according to the lower threshold (Bryers et al., 2013). Namely, the PDI is easily excited with the preexisting striation, and it dominates during the heating by taking advantage of the generation altitude. Except for the generation height, another reason the OTSI does not recover after overshoot is the high level of the electron temperature related to the OTSI excitation threshold, as mentioned above. Therefore, under high-ERP conditions, the HFPLs can reappear after overshoot, but the nonshifted HFILs cannot (Dhillon and Robinson, 2005; Mishin et al., 2016; Blagoveshchenskaya et al., 2017).

5. Summary

The overshoot phenomenon is a prominent feature in O-mode heating experiments. In this study, we have investigated the overshoot with experimental and simulation results, which give a clearer and more comprehensive understanding of the overshoot. At a lower ERP, the PDI and OTSI will be excited once the excitation thresholds of those instabilities are achieved, and they are immediately quenched by the fully established small-scale FAIs that contribute to the main overshoot observed in ISR spectra. In the simulation results, the competition between the PDI and OTSI leads to the pre-miniovershoot and the miniovershoot. After the overshoot, the reappearance of the PDI and the disappearance of the OTSI under high ERP are related to the occurrence height, the easier excitement of the PDI with the preexisting striation, and the OTSI excitation threshold, which depended on the electron temperature.

Acknowledgments

EISCAT is an international scientific association supported by research organizations in China (China Research Institute of Radiowave Propagation, CRIRP), Finland (Suomen Akatemia, SA), Japan (National Institute of Polar Research, and Institute for Space-Earth Environmental Research, NIPR and ISEE), Norway (Norges Forskningsrad, NFR), Sweden (Swedish Research Council, VR), and the United Kingdom (Particle Physics and Astronomy Research Council, PPARC). This work was supported by the National Natural Science Foundation of China (NSFC Grant Nos. 42104150, 42074187, 41774162, and 41704155), the Foundation of the National Key Laboratory of the Electromagnetic Environment (Grant No. 6142403200303), the Chinese Academy of Sciences, Key Laboratory of Geospace Environment, University of Science & Technology of China (Grant No. GE2020-01), the Fundamental Research Funds for the Central Universities (Grant No. 2042021kf0020), and the Excellent Youth Foundation of Hubei Provincial Natural Science Foundation (Grant No. 2019CFA054).

Data Availability

The experiments described in this paper were carried out by the Russian team led by N. F. Blagoveshchenskaya and the Norwegian team led by B. Gustavsson. The data used in this paper are available through the EISCAT database (https://portal.eiscat.se/). The simulation data are available from the ZENODO repository (https://doi.org/10.5281/zenodo.4745912).

References

Ashrafi, M., Kosch, M. J., Kaila, K., and Isham, B. (2007). Spatiotemporal evolution of radio wave pump-induced ionospheric phenomena near the fourth electron gyroharmonic. *J. Geophys. Res.: Space Phys.*, *112*(A5), A05314. https://doi.org/10.1029/2006JA011938

Blagoveshchenskaya, N. F., Borisova, T. D., and Yeoman, T. K. (2017). Comment on "Parametric instability induced by X-mode wave heating at EISCAT" by Wang et al. (2016). *J. Geophys. Res.: Space Phys.*, *122*(12), 36–49. https://doi.org/10.1002/2017JA023880

Bryers, C. J., Kosch, M. J., Senior, A., Rietveld, M. T., and Yeoman, T. K. (2013). The thresholds of ionospheric plasma instabilities pumped by high-frequency radio waves at EISCAT. *J. Geophys. Res.: Space Phys.*, *118*(11), 7472–7481. https://doi.org/10.1002/2013JA019429

Cannon, P. D., and Honary, F. (2015). A GPU-accelerated finite-difference time-domain scheme for electromagnetic wave interaction with plasma. *IEEE Trans. Antennas Propag.*, *63*(7), 3042–3054. https://doi.org/10.1109/TAP.2015.2423710

Chian, A. C. L., and Rizzato, F. B. (1994). Coupling of electromagnetic filamentation instability and electrostatic Langmuir parametric instabilities in laser–plasma interactions. *J. Plasma Phys.*, *51*(1), 61–73. https://doi.org/10.1017/S0022377800017396

Das, A. C., and Fejer, J. A. (1979). Resonance instability of small-scale field-aligned irregularities. *J. Geophys. Res.: Space Phys.*, *84*(A11), 6701–6704. https://doi.org/10.1029/JA084iA11p06701

Dhillon, R. S., and Robinson, T. R. (2005). Observations of time dependence and aspect sensitivity of regions of enhanced UHF backscatter associated with RF heating. *Ann. Geophys.*, *23*(1), 75–85. https://doi.org/10.5194/angeo-23-75-2005

Djuth, F. T., Isham, B., Rietveld, M. T., Hagfors, T., and La Hoz, C. (2004). First 100 ms of HF modification at Tromsø, Norway. *J. Geophys. Res.: Space Phys.*, *109*(A11), A11307. https://doi.org/10.1029/2003JA010236

DuBois, D. F., Hanssen, A., and Rose, H. A. (1992). Comment [on "Langmuir turbulence and ionospheric modification" by P. Stubbe, H. Kohl, and M. T. Rietveld]. *J. Geophys. Res.: Space Phys.*, *97*(A10), 15059–15066. https://doi.org/10.1029/92JA00904

Dubois, D. F., Hanssen, A., Rose, H. A., and Russell, D. (1993). Space and time

distribution of HF excited Langmuir turbulence in the ionosphere: Comparison of theory and experiment. *J. Geophys. Res.: Space Phys.*, *98*(A10), 17543–17567. https://doi.org/10.1029/93JA01469

Eliasson, B. (2008). Full-scale simulation study of the generation of topside ionospheric turbulence using a generalized Zakharov model. *Geophys. Res. Lett.*, *35*(11), L11104. https://doi.org/10.1029/2008GL033866

Eliasson, B., Milikh, G., Shao, X., Mishin, E. V., and Papadopoulos, K. (2015). Incidence angle dependence of Langmuir turbulence and artificial ionospheric layers driven by high-power HF-heating. *J. Plasma Phys.*, *81*(2), 415810201. https://doi.org/10.1017/S0022377814000968

Fejer, J. A. (1979). Ionospheric modification and parametric instabilities. *Rev. Geophys.*, *17*(1), 135–153. https://doi.org/10.1029/RG017i001p00135

Feng, T., Zhou, C., Wang, X., Liu, M. R., and Zhao, Z. Y. (2020). Evidence of X-mode heating suppressing O-mode heating. *Earth Planet. Phys.*, *4*(6), 588–597. https://doi.org/10.26464/epp2020068

Frolov, V. L., Sergeev, E. N., Komrakov, G. P., Stubbe, P., Thidé, B., Waldenvik, M., Veszelei, E., and Leyser, T. B. (2004). Ponderomotive narrow continuum (NC_p) component in stimulated electromagnetic emission spectra. *J. Geophys. Res.: Space Phys.*, *109*(A7), A07304. https://doi.org/10.1029/2001JA005063

Gustavsson, B., Newsome, R., Leyser, T. B., Kosch, M. J., Norin, L., McCarrick, M., Pedersen, T., and Watkins, B. J. (2009). First observations of X-mode suppression of O-mode HF enhancements at 6300 Å. *Geophys. Res. Lett.*, *36*(20), L20102. https://doi.org/10.1029/2009GL039421

Hagfors, T., Kofman, W., Kopka, H., Stubbe, P., and Äijanen, T. (1983). Observations of enhanced plasma lines by EISCAT during heating experiments. *Radio Sci.*, *18*(6), 861–866. https://doi.org/10.1029/RS018i006p00861

Kotov, P. V., Norin, L., Sergeev, E. N., Grach, S. M., and Thidé, B. (2007). Recovery of the ponderomotive parametric instability after long pumping of the ionosphere. *Adv. Space Res.*, *40*(3), 377–383. https://doi.org/10.1016/j.asr.2007.04.067

Kuo, S. P. (2021). Linear and nonlinear plasma processes in ionospheric HF heating. *Plasma*, *4*(1), 108–144. https://doi.org/10.3390/plasma4010008

Kuo, S. P., Lee, M. C., and Kossey, P. (1997). Excitation of oscillating two stream instability by upper hybrid pump waves in ionospheric heating experiments at Tromso. *Geophys. Res. Lett.*, *24*(23), 2969–2972. https://doi.org/10.1029/97GL03054

Kuo, S. P. (2001). Cascade of parametric instabilities in ionospheric heating experiments. *J. Plasma Phys.*, *66*(5), 315–336. https://doi.org/10.1017/S0022377801001477

Kuo, S. P. (2015). Ionospheric modifications in high frequency heating experiments. *Phys. Plasmas*, *22*(1), 01290. https://doi.org/10.1063/1.4905519

Lee, M. C., and Kuo, S. P. (1983). Excitation of upper-hybrid waves by a thermal parametric instability. *J. Plasma Phys.*, *30*(3), 463–478. https://doi.org/10.1017/S002237780000129X

Mahmoudian, A., Scales, W. A., Watkins, B. J., Bernhardt, P. A., Isham, B., Vega-Cancel, O., and Ruohoniemi, J. M. (2017). Investigation of third gyro-harmonic heating at HAARP using stimulated radio emissions and the MUIR and Kodiak radars. *Adv. Space Res.*, *59*(11), 337–350. https://doi.org/10.1016/j.asr.2016.09.029

Mishin, E., Watkins, B., Lehtinen, N., Eliasson, B., Pedersen, T., and Grach, S. (2016). Artificial ionospheric layers driven by high-frequency radiowaves: An assessment. *J. Geophys. Res.: Space Phys.*, *121*(4), 3497–3524. https://doi.org/10.1002/2015JA021823

Muldrew, D. B. (1988). Duct model explanation of the plasma line overshoot observed at Arecibo. *J. Geophys. Res.: Space Phys.*, *93*(A7), 7598–7604. https://doi.org/10.1029/JA093iA07p07598

Perkins, F. W., Oberman, C., and Valeo, E. J. (1974). Parametric instabilities and ionospheric modification. *J. Geophys. Res.*, *79*(10), 1478–1496. https://doi.org/10.1029/JA079i010p01478

Robinson, P. A. (1997). Nonlinear wave collapse and strong turbulence. *Rev. Mod. Phys.*, *69*(2), 507–574. https://doi.org/10.1103/RevModPhys.69.507

Robinson, T. R. (1983). *Modification of the High Latitude Ionosphere by High Power Radio Waves*. Leicester: University of Leicester.

Showen, R. L., and Kim, D. M. (1978). Time variations of HF-induced plasma waves. *J. Geophys. Res.: Space Phys.*, *83*(A2), 623–628. https://doi.org/10.1029/JA083iA02p00623

Streltsov, A. V., Berthelier, J. J., Chernyshov, A. A., Frolov, V. L., Honary, F., Kosch, M. J., McCoy, R. P., Mishin, E. V., and Rietveld, M. T. (2018). Past, present and future of active radio frequency experiments in space. *Space Sci. Rev.*, *214*(8), 118. https://doi.org/10.1007/s11214-018-0549-7

Stubbe, P., Kopka, H., Thidé, B., and Derblom, H. (1984). Stimulated electromagnetic emission: A new technique to study the parametric decay instability in the ionosphere. *J. Geophys. Res.: Space Phys.*, *89*(A9), 7523–7536. https://doi.org/10.1029/JA089iA09p07523

Stubbe, P., Kohl, H., and Rietveld, M. T. (1992). Langmuir turbulence and ionospheric modification. *J. Geophys. Res.: Space Phys.*, *97*(A5), 6285–6297. https://doi.org/10.1029/91JA03047

Stubbe, P. (1996). Review of ionospheric modification experiments at Tromsø. *J. Atmos. Terr. Phys.*, *58*(1-4), 349–368. https://doi.org/10.1016/0021-9169(95)00041-0

Thidé, B., Sergeev, E. N., Grach, S. M., Leyser, T. B., and Carozzi, T. D. (2005). Competition between Langmuir and upper-hybrid turbulence in a high-frequency-pumped ionosphere. *Phys. Rev. Lett.*, *95*(25), 255002. https://doi.org/10.1103/PhysRevLett.95.255002

Wu, J., Blagoveshchenskaya, N. F., Wu, J., Shen, X. H., Rietveld, M. T., Haggstrom, I., Xu, T., and Xu, Z. W. (2021). Altitude descents in high-frequency enhanced plasma and ion lines during ionospheric heating at EISCAT. *J. Atmos. Sol.-Terr. Phys.*, *212*, 105425. https://doi.org/10.1016/j.jastp.2020.105425

Wu, J., Wu, J., Rietveld, M. T., Haggstrom, I., Xu, Z., Zhang, Y., Xu, T., and Zhao, H. S. (2019). The intensities of high frequency-enhanced plasma and ion lines during ionospheric heating. *J. Geophys. Res.: Space Phys.*, *124*. https://doi.org/10.1029/2018JA025918